Available online at www.sciencedirect.com
SCIENCE DIRECT®
PERGAMON
International Journal of Heat and Mass Transfer 46 (2003) 3797–3808
International Journal of HEAT and MASS TRANSFER
www.elsevier.com/locate/ijhmt

A fundamental understanding of factors affecting frost nucleation

Byeongchul Na *, Ralph L. Webb

Department of Mechanical Engineering, The Pennsylvania State University, University Park, PA 16802, USA

Received 28 June 2002; received in revised form 4 April 2003

Abstract

Theoretical analysis of the nucleation process for frost formation on a cold surface shows that the air at the cold surface should be supersaturated in order for frost nucleation to occur. This understanding is new, relative to previously published frost growth models. Further, the supersaturation degree is dependent on the surface energy, which is related to the water contact angle. The theoretical predictions were compared to experimental results, and reasonable agreement was obtained. Qualitatively, a low energy surface (high contact angle) requires higher supersaturation degree for frost nucleation than a high energy surface. Quantitatively, the experimental data shows that the low energy surface requires approximately 10 times higher supersaturation degree than the high energy surface when the contact angle difference is approximately 80° at −20 °C surface temperature. The factors affecting the surface energy such energy such as temperature, surface roughness, and foreign particles are discussed in this paper.

1. Introduction

When air is cooled, moisture condensation (or freezing) may occur on the cold surface, and mass transfer will accompany the heat transfer. This occurs if the surface temperature of the cold surface is below the dew point temperature of the moist air. If the surface temperature is greater than the water freezing temperature, the condensed water vapor continuously drains along the evaporator surface. However, if the surface temperature is below the water freezing temperature, the transferred water vapor may either condense and then freeze, or desublimate (vapor-to-ice transformation) on the cold surface. The frost deposition continues until the frost surface temperature reaches the dew point temperature of the moist air.

Several authors have published theoretically based models to predict the growth of frost on a cold surface. Key models are Brian et al. [1,2], Jones and Parker [3], and Sami and Duong [4], who developed analytical models, and Le Gall and Grillot [5] who developed a numerical model. All of these models assume that the moist air at the frost surface is saturated at the temperature of the surface. These models all ignore the nucleation process of frost growth. Thus, they assume uniform growth of frost without the existence of a nucleation stage (or nucleation process). It is further known that the surface energy of the cold surface [6–8] will affect the nucleation process. Because the published models do not account for the nucleation process, they are also insensitive to the effects of surface energy on frost formation.

The key focus of this paper is to analytically address the initial frost nucleation and the factors that affect it—including the surface energy of the base surface, which may be altered by surface treatment.

Frost formation on a cold surface involves two distinct processes: nucleation and crystal growth [6,7]. The initial frost deposition on a cold surface involves a nucleation process. The nucleation process requires that the embryo to overcome the Gibbs energy barrier, and this can be achieved by the supersaturation of the phase changing substance [6].

* Corresponding author. Tel.: +1-814-865-9719; fax: +1-814-865-1344.
E-mail addresses: bxn6@psu.edu (B. Na), r5w@psu.edu (R.L. Webb).

0017-9310/03/$ - see front matter © 2003 Elsevier Ltd. All rights reserved.
doi:10.1016/S0017-9310(03)00194-7

Nomenclature

A	area [m^2]
G	Gibbs free energy [J]
g	Gibbs free energy per unit volume [J/m^3]
I	embryo formation rate
I_0	the kinetic constant for embryo formation, 1.38066×10^{-23} [J/K]
H	enthalpy of system [J]
Δh	latent heat [kJ/kg]
k	Boltzmann constant, 1.38066×10^{-23} [J/K]
m	cosine of contact angle
P_v	vapor pressure [kPa]
r	radius of embryo [m]
S	entropy of total system [kJ/K]
SSD	supersaturation degree defined by Eq. (8), non-dimensional
s	entropy per unit volume [kJ/m^3 K]
T	temperature [°C]
T_K	temperature [K]
V	volume [m^3]

Greek symbols

γ	surface energy [kJ/m^2, mJ/m^2]
θ	contact angle [degree]
ρ	density [kg/m^3]
σ	interfacial energy [kJ/m^2, mJ/m^2]

Subscripts

A	air
cr	critical value
fs	frost surface
i	parent phase
j	new phase
l	liquid
v	vapor
sat	saturation state
super	super cooled state
s	solid, substrate
w	wall

Other symbols

-	(over-bar) average value
$\sim$	physical quantity per unit volume

Sanders [7] considered why frost does not uniformly form on a cold surface and concluded that the inhomogeneity of surface energy affects the sites of frost initiation. However, he did not analytically develop the surface energy effect. Although he realized that the surface energy affects the frost initiation, he assumed in his frost growth model that frost starts to form when the air is saturated at the cold surface temperature. This will overpredict the frost growth rate because the frost initiation will be delayed on a low energy surface. Hayashi et al. [9] proposed the morphology of crystal growth during the initial stage of frost formation on a cold surface; but he did not mention or consider the nucleation process.

It is necessary for the air to be supersaturated for frost nuclei to form. Even after nucleation has occurred and a very thin frost layer exists, supersaturation at the surface is still required for frost growth. This is because frost growth also involves a nucleation process. The previously referenced models, which assume saturated conditions at the interface, will overpredict the mass transfer driving potential. The analysis to be presented here shows that the assumption that the air is saturated at the frost surface results in over-prediction of the mass transfer rate. Typically, this over-prediction is in the range of 20% of the total mass transfer rate. The detailed analysis is in Appendix A, because this paper focuses on the nucleation process on a cold surface.

Further, the surface energy of the base surface will affect the initial frost nucleation. However, after a thin frost layer is deposited, the surface energy of the base surface no longer affects the frost nucleation process. No publications were found that account for the nucleation process in frost growth models. Even empirical models [10–12] based on experiment do not account for the surface energy of the base surface on frost initiation. The assumption of the saturation state when frosting starts, used in all of the referenced publications, does not recognize the necessity of supersaturation degree related to the nucleation process.

The Gibbs free energy required for nucleation is influenced by the surface energy, which is related to contact angle. A low energy surface (high contact angle) will require higher supersaturation for nucleation than will be required for a high energy surface (low contact angle) [6–8]. Surface roughness or coatings can alter the surface energy. This work also addresses the effect of surface energy of the base surface on the initial frost nucleation process. The predicted results will be compared to experimental measurements. Finally, the implication of the results will be discussed.

For the development of a complete frost growth model, one would use the presently developed model until a very thin layer is developed. Then the frost growth would be based on model similar to that of those referenced above, but modified to account for super-

saturation at the frost surface. This model is described by Na [13].

2. Thermodynamitical analysis of nucleation

2.1. Nucleation

The nucleation process requires that the vapor embryo overcome a certain Gibbs energy barrier [6]. This vapor embryo is a concentration of water molecules that are transformed to a frost nucleus. Although the cooled, moist air may be saturated at the cold surface, frost nucleation will not occur, unless the Gibbs energy barrier is exceeded. For nucleation to occur, the vapor will be in a supersaturated, metastable state—not the saturated state. The Gibbs energy change required for nucleation is referenced to the saturation state, and the symbol Δ in the equations given here means the difference between the supersaturated state and saturated state.

The Gibbs energy change of the embryo contacting the cold surface is given by the following equation [6]:

$$\Delta G = V_{\text{embryo}}\Delta\tilde{g}_{\text{v}} + A_{\text{ij}}\sigma_{\text{ij}} + A_{\text{js}}(\sigma_{\text{js}} - \sigma_{\text{is}}) \tag{1}$$

Fig. 1a explains each symbol in Eq. (1). The σ symbols represent the interfacial energy, and the A's are the contact areas between each substance (or surface). The interfacial energy is a function of temperature, because the interfacial energy is related to the surface energy of the substance [14], and the surface energy is dependent on temperature [15]. Sanders [7] gives the interfacial energy between water vapor and water, water and ice, and water vapor and ice, and the equations for these interfacial energies are given in Table 1. The symbol V represents the volume of the new phase, which is the nucleus for crystal growth. The subscripts 'i', 'j', and 's' represent the parent phase, new phase, and the substrate on which the phase change occurs, respectively. The symbol $\Delta\tilde{g}_{\text{v}}$ is the Gibbs energy change between the parent phase and the new phase per unit volume and is dependent on the temperature change and vapor pressure. The symbol G is the Gibbs energy defined by

$$G \equiv H - T_{\text{K}}S \tag{2}$$

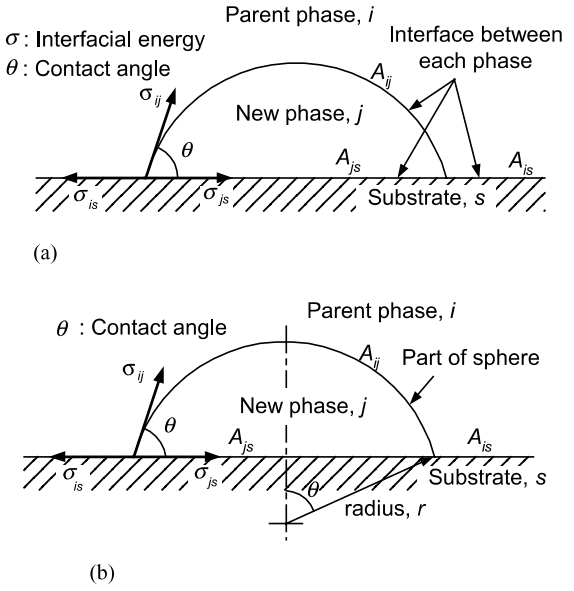

Fig. 1. Contact angle and Fletcher's heterogeneous nucleation model: (a) explanation of the contact angle and related parameters (b) Fletcher's heterogeneous nucleation model.

Therefore, the Gibbs energy change $\Delta\tilde{g}_{\text{v}}$ between the parent phase and the new phase during the phase change can be expressed as

$$\Delta\tilde{g}_{\text{v}} = \Delta\tilde{h}_{\text{latent}} - T_{\text{K}}\Delta\tilde{s}_{\text{latent}} \tag{3}$$

The latent entropy $\Delta\tilde{s}_{\text{v}}$ is given in Table 1 and is calculated using the Clapeyron equation.

As shown in Eq. (1), the Gibbs energy change is related to the interfacial energy between substances. Therefore, the surface energy of the cold surface, which is related to the interfacial energy, is an important parameter for heterogeneous nucleation—nucleation between metastable moist air and a solid surface. For homogeneous nucleation, the last term on the right side in Eq. (1) is excluded.

In order to thermodynamically analyze the nucleation process, Fletcher [6] and Sanders [7] assumed the shape of the parent phase for the nucleation is a spherical segment as shown in Fig. 1b. The Gibbs energy change of the embryo will change with the size of the

Table 1
Constant and equations for calculating the initiation of nucleation [6]

Phase change	State		I_0 (/m^2 s)	Interfacial energy, σ_{ij} (kJ/m^2)	$\Delta\tilde{s}_{\text{latent}}$ (kJ/m^3 K)
	i	j			
Condensation	Vapor	Water	10^{29}	$\sigma_{\text{ij}} = (75.7 - 0.1775T) \times 10^{-6}$	$(\Delta h_{\text{lv}}/T_{\text{K}})\rho_{\text{l}}$
Desublimation	Vapor	Ice	10^{29}	$\sigma_{\text{ij}} = (99.5 - 0.075T) \times 10^{-6}$	$(\Delta h_{\text{sv}}/T_{\text{K}})\rho_{\text{ice}}$
Freezing	Water	Ice	10^{32}	$\sigma_{\text{ij}} = (23.8 + 0.1025T) \times 10^{-6}$	$(\Delta h_{\text{ls}}/T_{\text{K}})\rho_{\text{ice}}$

embryo, and the critical Gibbs energy change can be calculated by differentiating Eq. (1) with respect to the radius of the embryo. Using the Fletcher model, the critical Gibbs energy change can be obtained at the critical embryo size (r_c).

$$\Delta G_c = \frac{16\pi}{3}\frac{\sigma_{ij}^3}{\Delta\tilde{g}_v^2}\frac{(2+m)(1-m)^2}{4} \tag{4}$$

$$r_c = -\frac{2\sigma_{ij}}{\Delta\tilde{g}_v} \tag{5}$$

where m is the cosine of the static contact angle θ in Fig. 1b.

$$m \equiv \cos\theta = \frac{\sigma_{js} - \sigma_{is}}{\sigma_{ij}} \tag{6}$$

Eqs. (1)–(4) assume that the base surface is perfectly smooth. If the surface is rough, the contact angle does not represent the precise interfacial energy because the roughness affects the contact angle [8,16].

Becker and Doring [16] have given the following equation for estimating the embryo formation rate on a unit surface area for heterogeneous nucleation, and in a unit volume for homogeneous nucleation:

$$I = I_0 \exp\left(-\frac{\Delta G_c}{kT_K}\right) \tag{7}$$

The symbol I is the embryo formation rate, I_0 is the kinetic constant shown in Table 1, and k is the Boltzmann constant (1.38066×10^{-23} J/K). The temperature T_K is the surface temperature given in Kelvin.

Using Eqs. (4)–(7), the embryo formation rate can be calculated, and the result calculated at 0 °C wall temperature is shown in Fig. 2. As the water vapor pressure increases, the Gibbs energy change of the water vapor in a given volume, $\Delta\tilde{g}_v$ (Eq. (4)) increases because of the high density of the water vapor, and the critical Gibbs energy change of the embryo decreases. This causes the embryo formation rate to increase according to Eq. (7). From Eq. (4), the critical Gibbs energy change of the embryo increases as the contact angle on the surface increases. This means that relatively low embryo formation rate will exist for high contact angle (a low energy surface), as compared to that for low contact angle.

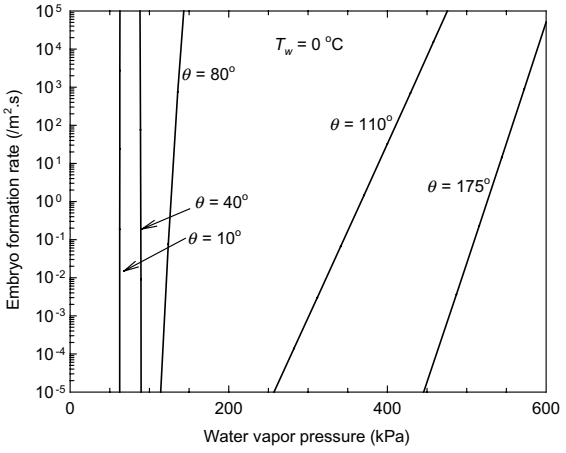

Fig. 2. Embryo formation rate ($T_w = 0$ °C).

Many investigations have been conducted for nucleation and showed the above Becker–Doring theory is in good agreement with experimental findings [16]. Also, it was found that the critical embryo formation rate exists for nucleation. Experiments by Volmer and Flood showed that homogeneous nucleation of water vapor starts when $\ln I \approx 10/\mathrm{m}^2\,\mathrm{s}$ [16]. This means that there exists a threshold embryo formation rate for nucleation.

2.2. Supersaturation

As described in the previous section, for phase change the parent phase must overcome the Gibbs energy barrier. From Eq. (7), the embryo formation rate increases as the critical Gibbs energy decreases. The critical Gibbs energy change is dependent on the interfacial energy at each interface, and the Gibbs energy change of the water vapor per unit volume, as shown by Eq. (4). The Gibbs energy change of the water vapor per unit volume occurs in two ways: (1) water vapor pressure change or (2) temperature change. For the Gibbs energy to change, the water vapor pressure must be higher than the saturated state, or the surface temperature must be lower than the saturation temperature. These two criteria mean that the water vapor must be supersaturated at a given condition for the nucleation. However, as previously noted, models for frost formation on cold surfaces assume that the frost forms when the surface temperature reaches the dew point temperature. The present model is in disagreement with the usually taken assumption.

Sanders [7] and Harraghy and Barber [17] define supersaturation degree as

$$\mathrm{SSD} \equiv \frac{P_v - P_{v,sat}}{P_{v,sat}} \tag{8}$$

where P_v is the local vapor partial pressure of the air, and $P_{v,sat}$ is the saturated vapor pressure at the same point.

The difference between condensation and desublimation, below the water freezing temperature, will be explained in the next section. As shown in Fig. 3, for the water vapor to change its phase and deposit frost on a cold surface, the water vapor must be supersaturated at the cold surface temperature. Also, the extent of the supersaturation is strongly dependent on the surface energy represented by the surface contact angle. This implies that the frost deposition can be delayed by

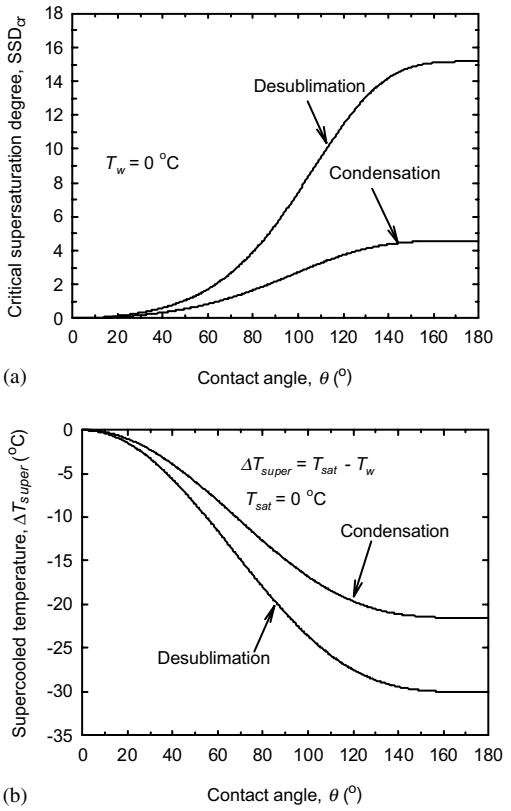

Fig. 3. Predicted supersaturation phase change limits vs. contact angle: (a) critical supersaturation degree ($T_w = 0$ °C) (b) condensation and desublimation temperature ($T_{sat} = 0$ °C).

controlling the surface energy. Therefore, by using a low surface energy coating on the surface, it may be possible to maintain the surface frost-free within a specific range.

2.3. Condensation and desublimation

The phase change of water vapor below the water freezing temperature may occur by two mechanisms: (1) condensation to water and freezing to ice, (2) desublimation to ice. From Eq. (4), the critical Gibbs energy change is dependent on the interfacial energy between the parent phase and new phase, as well as the interfacial energy and Gibbs energy change of water vapor. Table 1 shows that the interfacial energy between water vapor and water is smaller than that between water vapor and ice. This means that the critical Gibbs energy for condensation is smaller than that for desublimation, and that the embryo formation rate is larger for condensation than for desublimation. Therefore, the condensation process is favorable to the phase change of water vapor at the low water vapor pressure. And at high vapor pressure, both condensation and desublimation processes are favorable to phase change of the water vapor.

Supersaturation of the water vapor can be achieved by two methods: (1) increase in the vapor pressure above the saturated vapor pressure at a given wall temperature, (2) decrease in the wall temperature at a given water vapor pressure. Fig. 3a shows the critical supersaturation degree (SSD_{cr}) and phase change limits for condensation and desublimation at 0 °C wall temperature. Fig. 3b shows similar information for $T_{sat} = 0$ °C with the required supercooling of the surface defined as $\Delta T_{super} = T_{sat} - T_w$. Due to the difference of the interfacial energy between water and ice, Fig. 3 shows different limits for condensation and desublimation. The calculations use the embryo formation rate of $\ln I \approx 10/m^2\,s$ from the Volmer and Flood [16] experimental investigation for homogeneous nucleation.

2.4. Position of nucleation

When moist air is cooled by a cold surface, some portion of the moist air near the wall may be already supersaturated before frosting on the cold surface, because of the temperature gradient in the air. Therefore, it is meaningful to analyze whether the frost forms only on the cold surface, or if frost can also be formed in the air at the cold surface.

In the previous sections, the heterogeneous nucleation process was analyzed. However, considering the case for 180° contact angle, homogeneous nucleation can be explained. In Eq. (4), when the value of m (the cosine of the contact angle) is -1, the equation describes homogeneous nucleation, and the critical Gibbs energy change has the maximum value at a given condition.

When moist air is cooled by the cold surface, the lowest temperature in the air occurs at the cold surface. Before starting nucleation, the supersaturation degree is highest at the wall. Due to the previous two reasons, frost nucleation will occur only on the cold surface, when the moist air is cooled by the cold surface.

Summarizing the nucleation process:

(1) For phase change nucleation, a threshold embryo formation rate exists. This requires supersaturation of the water vapor for the phase change.
(2) The embryo formation rate is dependent on the water vapor pressure, surface energy, and surface temperature.
(3) A lower energy surface causes lower embryo formation rate in a given condition. Therefore, the frost formation will be delayed on the lower energy surface.
(4) Below the water freezing temperature, water vapor can change its phase to ice on a cold surface by desublimation or by freezing following condensation.

Although condensation occurs on the cold surface, only the ice phase will exist on the surface, because the condensed water immediately freeze after condensation.

(5) The nucleation of frost in the system composed of the moist air and the cold surface starts on the cold surface—not in the moist air.

In the next sections, the thermodynamic analysis for frost formation will be compared to the experimental data, and the implication of the findings will be discussed.

3. Experimental method

3.1. Experimental apparatus and test procedure

A low temperature wind tunnel was used for the investigation of the frost formation. Fig. 4 shows the schematic of the low temperature wind tunnel. The humidity of the moist air was adjusted in the control chamber by controlling the heat exchanger temperature. The humidity was calculated by measuring the temperature of the air leaving the control chamber, because the air is saturated in the control chamber. The surfaces of interest were installed in the test section, and cooled by a thermoelectric module, from which the heat was removed by a refrigeration system. For the test, the humidity in the wind tunnel was controlled to the set value, and then the surface in the test section was slowly cooled down.

The observed frost pattern on the surface was not homogeneous, which means that the frosting started at discrete points and some regions were unfrosted to a certain surface temperature drop during the test. The observed frosting during one test, is shown in Fig. 5, for which $T_w = -20$ °C. Due to the inhomogeneity of the frosting pattern, the data recording was conducted as follows:

- The frost initiation on the surface was observed while the temperature of the cold surface is cooled down. When the first spot of the frost was observed, the temperature of the cold surface was recorded.
- The plate temperature was further slowly reduced, until the frost covered approximately 80% of the cold surface, the temperature was recorded.

3.2. Test surfaces

3.2.1. Preparation of surfaces

In order to investigate the effect of the surface energy on the nucleation of the frost, five kinds of surfaces were prepared for the test:

- *Boehmite treated surface*. Water was boiled in a stainless steel pot, and then the aluminum surface was immersed into the boiling water for 30 min. The boiled aluminum plate was cleaned by the flowing cold water and then dried. The Boehmite process is described by Min and Webb [18].
- *Bare aluminum*. The buffed and cleaned aluminum surface was used for the bare surface.
- *Transparent polymer packaging tape on the aluminum surface*. The adhesive backed transparent packaging tape was attached to the bare surface.
- *Silicone wax coated aluminum surface*. An automobile wax containing silicone was coated on the bare surface. This provided a hydrophobic characteristic [19].

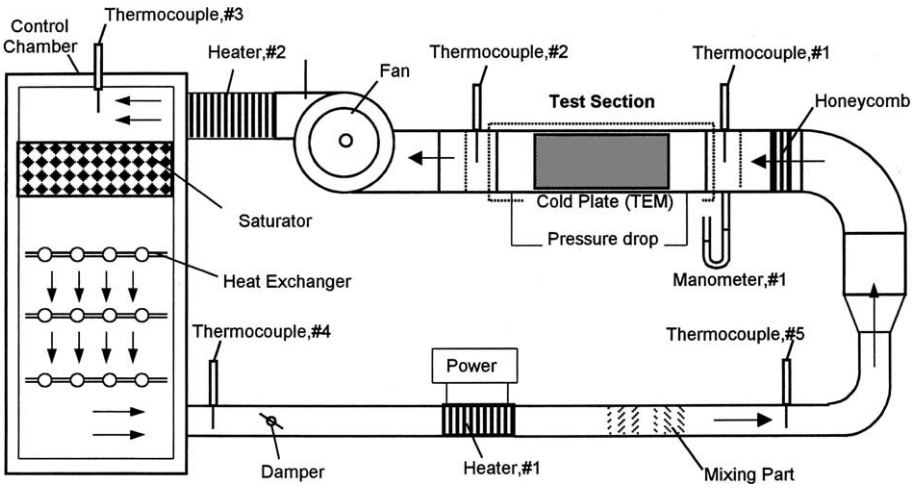

Fig. 4. Low temperature wind tunnel.

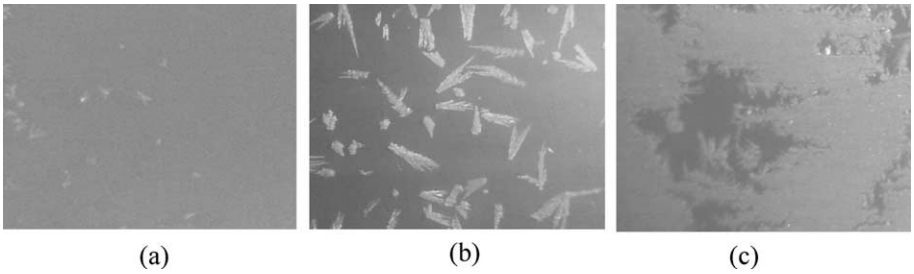

Fig. 5. Frosting shape on the cold surface ($T_w = -20$ °C): (a) initiation frost; (b) growth of frost and (c) covering the surface.

- *Teflon coated aluminum surface*. A Teflon emulsion was sprayed on the aluminum surface and sintered at 360 °C for 40 min.

3.2.2. Measurement of contact angle

The static contact angle on each surface was measured by the sessile drop method using a Rame–Hart Model 100 goniometer of which the resolution is 1°. Because of non-linear relation between the contact angle and the required supersaturation degree, it is not practical to relate the goniometer resolution to the supersaturation degree. The contact angle on each surface was measured three times: (1) after surface treatment, (2) after test, (3) after test and drying the surfaces. In each measurement, the measured values at five points on the same surface were averaged.

4. Results and discussion

4.1. Contact angle results

Fig. 6 shows the results of the measured contact angles (static, advancing, and receding) on the different surfaces. Different results are shown for the static, advancing, and receding contact angle measurements. The difference between the advancing contact angle and receding contact angle is called contact angle hysteresis. Attention is first directed at the static contact angle results to assess the effect of surface energy on nucleation. The surface energy is a static property of the surface. As previously noted, each reported contact angle was measured at five points on the same surface and averaged. The standard deviations of the measured contact angles on the surface were less than 7% of the averaged values at each dry and wet surface. Fig. 6 shows contact angle measurements for three different test conditions: (1) after surface treatment, but before frost deposition (S1), (2) after frost deposition and after melting the frost and drying the surface (S2), and (3) after drying the surface at 100 °C for 40 min.

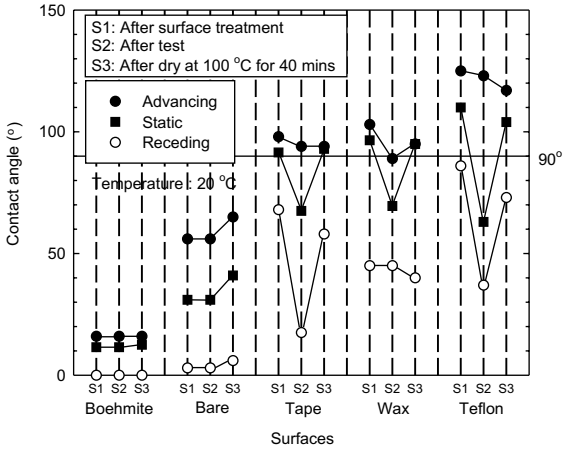

Fig. 6. Contact angle on the different surfaces.

The S1 data set show that the Boehmite treated surface and the bare surface have a hydrophilic characteristic (small contact angle), and the other surfaces show a hydrophobic characteristic (large static contact angle) after surface treatment. However, after the frosting test, the S2 data set show that the contact angle of the hydrophobic surfaces decreases by 20–40°. While testing with frost formation, the surfaces may be contaminated by the deposition of foreign particles such as dust in the air stream, and adsorption of the water vapor. This contamination affects the surface energy, which is represented by the contact angle. Although it is not practical to remove the spurious foreign particles on the surfaces, the effect of the water vapor can be verified by removing the water vapor by heating the surfaces.

The S3 data set (surfaces were dried at 100 °C for 40 min and then cooled to room temperature) show the effect of adsorption of water vapor on the change of the contact angle. Fig. 6 shows that the contact angle was recovered after drying, and that the adsorption of the water vapor seriously affects the contact angle by changing the surface energy for the hydrophobic surfaces after the surface treatment. For the bare aluminum surface, the static contact angle increased when the surface was dried. This result may be due to oxidization

occurring during the drying process. It was also found that the contact angle on the Boehmite treated surface is not affected by water vapor adsorption. The Boehmite treatment hydrates the aluminum oxide formed by the surface treatment and generates a micro-roughened oxidation layer on the aluminum surface [18], which yields low contact angle. If the micro-roughness alone affects the water contact angle, other factors such as the adsorption of the water vapor will not be effective in altering the contact angle. Because the contact angle does not change after drying the surface, it is concluded that the micro-roughness alone affects the contact angle. This result is in good agreement with the result of Min and Webb [18].

The phenomenon that a difference between the advancing and receding contact angle exists is called contact angle hysteresis. Although the phenomenon of contact angle hysteresis is not fully understood, it is known that the surface heterogeneity such as surface roughness and impurity is attributed to the hysteresis [16]. As shown in Fig. 6, the differences between the advancing and receding contact angle for the Boehmite treated surface and bare surface do not change after the test. This shows that the water vapor adsorption is not significant on these surfaces. However, for the polymer tape and Teflon surfaces, the differences became larger after the test, and after drying the surfaces, the differences were recovered to the values measured before testing. From this result, it is also indirectly proved that water vapor was adsorbed on the polymer surfaces and increased the surface heterogeneity. For the waxed surface, the trend is opposite to those of the other polymer surfaces. The car wax is a compound of several components for its own purpose, and this might affect the hysteresis characteristic. The analysis of this effect is beyond of the scope of this paper.

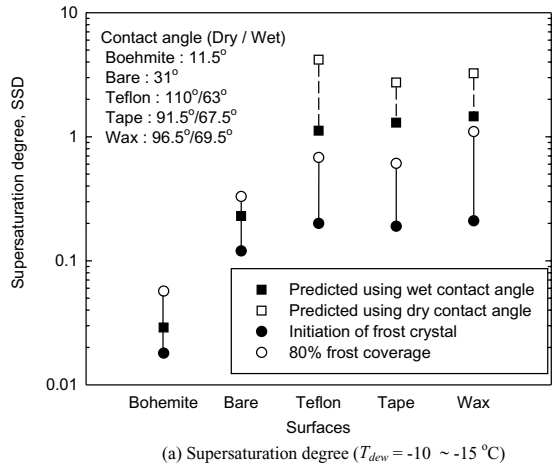

(a) Supersaturation degree (T_{dew} = -10 ~ -15 °C)

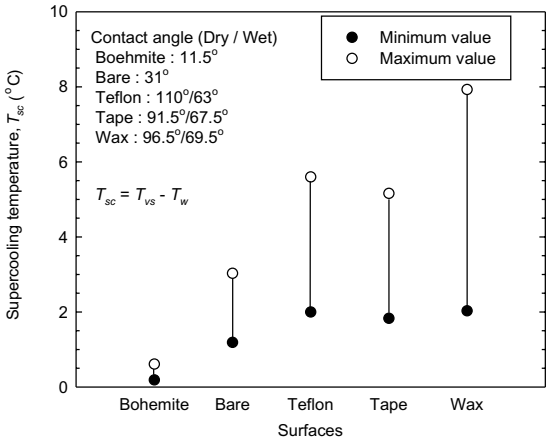

(b) Supercooling temperature (T_{dew} = -10 ~ -15 °C)

Fig. 7. Experimental results: (a) supersaturation degree (b) supercooling temperature.

4.2. Initiation of frost on cold surfaces

Initiation of frost formation was observed on the five different surfaces, and the humidity and frosting temperature were recorded. Fig. 7 shows experimental and predicted values of the supersaturation degree. The supersaturation degree test was conducted four or five times for each surface, and the value varies less than 10%. The experimental values are shown for the initiation of the frosting, and for 80% frost coverage on the surface. Using the transparent graph paper of which resolution is 1 mm, the frosted area was marked, and the ratio of the frosted area to the total area was calculated. The predicted values are for the required supersaturation degree based on thermodynamic analysis given in Section 2.1. The predicted values were based on two static contact angle measurements—one after surface treatment and before frosting (S1 from Fig. 6), which is designated dry contact angle, and the other after the frosting test (S2 from Fig. 6), which is called wet contact angle, because of the water adsorption.

Fig. 7 test results show that the low energy surfaces having higher contact angle require high supersaturation degree for nucleation, which is in agreement with the thermodynamic nucleation analysis. The detailed observations are as follows.

4.2.1. Incipient nucleation and active nucleation

The experimental results show a difference between the supersaturation degree for "incipient nucleation" (defined as the onset of frost) and "active nucleation" (defined here as 80% frost coverage). The supersaturation degree is smaller for incipient nucleation. The difference of the supersaturation degree between incipient nucleation and active nucleation may occur due to the inhomogeneity due to the partial contamination or roughness difference of the surface. This means that the

local surface energy is different on the surface, and the frost formation initiates at the highest points of surface energy. With increasing air humidity, the other sites become active to the frost formation. This inhomogeneity is apparently caused by surface roughness, contamination, and adsorption of the water vapor.

4.2.2. Agreement with the theoretical analysis

The predicted values using the wet contact angle are representative of the surface energy of a surface, because the water vapor will be adsorbed into the surface before frosting starts. Carey [8] discusses the effect of the water vapor adsorption on a surface for dropwise condensation on a cold surface. He proposes that the adsorbed water vapor provides nuclei for condensation. This phenomenon can also occur in the frost formation process, and will accelerate the frost formation. This may be why the predicted values show better agreement with the contact angles measured after surface treatment than those measured after frosting. Because the contact angle is greater after surface drying proves that adsorption of water vapor occurred.

Fig. 7 shows the range of the supersaturation degree from frost incipience to 80% coverage of frost. The frost coverage on the surface can be explained in two ways. One is that the surface is covered by the frost initiated on that point. The other is that the surface around the frost inception points is covered by the frost grown from the incipient points. This can be observed from the frost propagation shape in Fig. 5b. Once incipient frost formation occurs, two frost formation sites exist on the surface—one is the cold surface and the other is the frost itself. The water vapor on the frost crystal grows the crystal size 3-dimensionally. Around the incipient nucleation sites, the frost formation on the frost crystal is more favorable rather than on the cold surface, because the surface energy on the frost crystal is larger than on the surface. Hence, although frost does not form on the surface around the incipient sites, the surface can be seen covered by the frost grown from the incipient sites. Therefore, it is difficult to define when all of the surface is active for the frost formation. In this work, when the frost covers the surface approximately 80% of the total surface, the surface is arbitrarily assumed active to frost formation.

The theoretical prediction using wet contact angle is in agreement with the measured supersaturation degree within 30%. However, still the theoretical model overpredicts the experimental results. This overprediction is discussed below.

4.2.3. Overprediction of theoretical analysis

Generally, these theoretical values (using wet angle) overpredict the experimental results for 80% frost coverage. This is primarily because the contact angles were measured at room temperature and the experimental values were measured at −20 °C, as discussed below.

Also, foreign particles that settle onto the surface from the air flow may be nuclei for frost formation. If the foreign particles have higher surface energy than that of the original surface, the frost formation starts earlier than on the original surface.

Surface roughness will also affect the nucleation process. Eq. (1) shows that the Gibbs energy change increases as the contact area between the embryo and the substrate increases. As shown in Fig. 8, when the embryo forms on the peak or valley of the roughness, the contact area is larger than when the embryo forms on a perfectly smooth surface. This roughness effect will reduce the supersaturation degree compared to the predicted values.

The phenomenon of incipient and active frost formation on a heterogeneous is similar to that of nucleation pooling boiling. In pool boiling, vapor nuclei must exist in the heterogeneous sub-surface structure. The required superheat degree for vapor nuclei depends on the surface characteristics such as surface roughness (or sub-surface micro-structure) and the contact angle. For pool boiling, the liquid must be superheated for a vapor nucleus to exist.

The surface energy of solid metal surfaces and organic materials is temperature dependent. Van der Waals and Guggenheim [15] proposed the following equation for the surface energy:

$$\gamma = \gamma^0(1 - T/T_c)^n \tag{9}$$

where γ is the surface energy, γ^0 the surface energy at 0 K, T_c the critical temperature and n is approximately unity for metal, and slightly larger than unity organic material.

The Van der Waals and Guggenheim equation shows that the surface energy increases as the temperature decreases. This means that the surface energy changes with the change of surface temperature, which changes the interfacial energy.

The frequently used approaches to calculate the interfacial energy using surface energies are the "equation of state approach" and "surface tension components approach" [14]

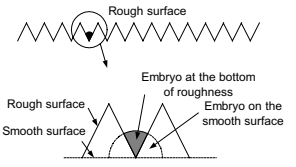

Fig. 8. Effect of roughness on the embryo contact area.

Equation of state approach:

$$\sigma_{js} = \gamma_j + \gamma_s - 2\sqrt{\gamma_j\gamma_s}e^{\beta(\gamma_j-\gamma_s)^2} \quad \text{where}$$
$$\beta = 0.0001247(m^2/mJ)^2 \tag{10}$$

Surface tension components approach:

$$\gamma_s = \frac{\gamma_j(1+\cos\theta)^2}{4} \quad \text{where } \cos\theta = \frac{\sigma_{js}-\gamma_s}{\gamma_j} \tag{11}$$

However, Balkenende et al. [14] found that neither of the above two approaches accounts for all experimental data on low energy surfaces, and that the surface tension component approach is only appropriate available for apolar surfaces. However, the above two equations show that the interfacial energy increases as the surface energy increases. In this work, the contact angle was measured at room temperature, and the frosting test was conducted at a cold surface temperature of approximately −20 °C. This means that the interfacial energy between the substrate and new phase at the frosting temperature increased due to the increased surface energy of the substrate. The increased interfacial energy reduced the supersaturation degree for frost formation, and this may be one of reasons that the prediction results overpredict the supersaturation degree compared to the experimental data.

5. Conclusions

(1) The nucleation process for the incipient frost formation was analyzed based on thermodynamic principles.
(2) For frost formation to occur, the air at the cold surface must be supersaturated.
(3) Lower energy surfaces require higher supersaturation degree for nucleation than do higher energy surfaces.
(4) The inhomogeneity of the surface energy causes a heterogeneous frosting pattern, because the required supersaturation degree for the nucleation locally differs.
(5) Surface roughness reduces the required supersaturation degree.
(6) This work suggests the possibility of developing surfaces that delay frost formation to lower surface temperature.

Appendix A. 2-Dimensional nucleation

In contrast to the nucleation of frost on a bare cold surface, the nucleation on a surface of frost crystals is 2-dimensional, because water vapor forms an island (a 1-molecule thick, flat layer) on the crystal surface [6]. The successive nucleation on the frost crystal makes the frost crystal and the frost layer grow. For a 3-dimensional nucleation process, which is on a foreign surface, Eq. (1) gives ΔG. However, for a 2-dimensional nucleation process, the equation for ΔG is given by [6]

$$\Delta G = \pi r^2 a\Delta\tilde{g}_v + 2\pi r a\sigma_{ij} \tag{A.1}$$

$$\Delta G_c = -\frac{\pi\sigma_{ij}^2 a}{\Delta\tilde{g}_v} \tag{A.2}$$

$$r_c = -\frac{\sigma_{ij}}{\Delta\tilde{g}_v} \tag{A.3}$$

where the symbol a is the diameter of the water vapor molecule, and r is the radius of the island, which is the cylindrical shape perpendicular to the frost crystal surface. In this cylindrical shape, the energy due to the interfacial energy only exists at the peripheral surface of the cylinder. Therefore, the last term in Eq. (1) vanishes, and the Gibbs energy change of the embryo for the 2-dimensional nucleation is expressed as Eq. (A.1).

Using Eqs. (A.2) and (7), the required supersaturation can be calculated analogous to the procedure described in Section 2.1. It is noted that Eq. (A.1) does not include the cold surface energy, and that the Gibbs energy change for nucleation is only dependent on the temperature. Fig. 9 shows the required supersaturation degree for frost nucleation on the frost surface. In this analysis, the diameter of water vapor molecule was assumed to be 1 Å. From this analysis, it is found that the water vapor at the frost surface should be supersaturated for the frost crystal to grow. Therefore, while the frost crystal is growing, the water vapor pressure at the frost surface is supersaturated. Because the water vapor at the frost surface is supersaturated, the driving potential for the mass transfer from the air stream to the

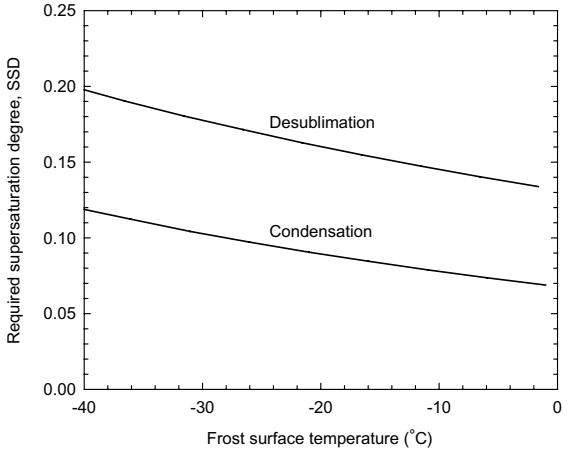

Fig. 9. Required supersaturation degree on the frost crystal surface.

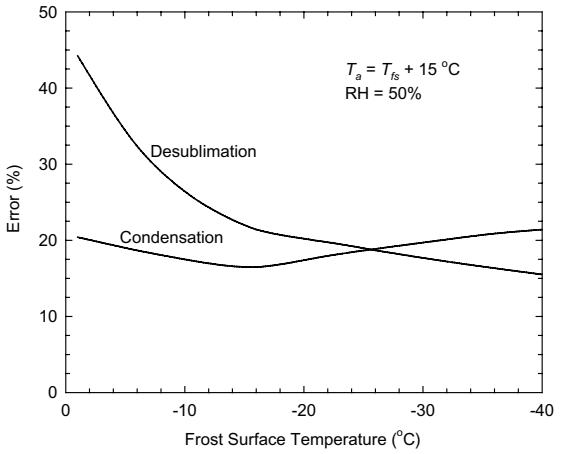

Fig. 10. Analysis of error in mass transfer rate caused by the assumption that the air is saturated at the frost surface.

frost surface is smaller than the value calculated with the assumption that the air is saturated at the frost surface.

Fig. 10 shows an example calculation for the error in predicting the mass transfer rate occurring when assuming the air is saturated at the frost surface. This calculation is performed for air at 50% relative humidity, and the surface temperature is 15 °C below the air temperature. The calculated error shown in Fig. 10 is the minimum value, because the minimum (required) supersaturation degree for nucleation was used. The error in Fig 10 is defined as

$$\text{Error}(\%) = \frac{\Delta P_{w,2} - \Delta P_{w,1}}{\Delta P_{w,1}} \times 100 \tag{A.4}$$

where ΔP_w is the vapor pressure difference between the air stream and the frost surface. Symbol $\Delta P_{w,1}$ is for supersaturation at the frost surface, and $\Delta P_{w,2}$ assumes the air is saturated at the frost surface temperature.

Fig. 10 shows that the assumption of saturated conditions at the frost surface will result in over prediction of the mass transfer rate in the range of 20%. For desublimation significantly higher over prediction can exist at frost temperatures near 0 °C.

A.1. Example calculation for mass transfer rate

Conditions. Air flows over the frost surface on a flat plate. The air free stream temperature is −5 °C, and 50% relative humidity. The frost surface temperature is −20 °C.

Properties. Water vapor pressure in the air stream, $P_{v,a}$ at −5 °C and RH 50%: 0.2009 kPa. Saturated water vapor pressure at the frost surface temperature: 0.1033 kPa.

Calculation. The mass transfer rate can be calculated by [20]

$$m'' = K_p(P_{v,a} - P_{v,fs}) \tag{A.5}$$

where K_p is the mass transfer coefficient defined based on the vapor pressure difference, and $P_{v,a}$ and $P_{v,fs}$ are the water vapor pressures in the air flow and frost surface, respectively.

For −20 °C frost surface temperature, Fig. 9 shows that $SSD_w = 0.17$ is the theoretical limit for the nucleation on the frost crystal surface. For this example, we have used $SSD_w = 0.20$. The water vapor pressure at the frost surface is calculated using supersaturation degree.

$$SSD_w \equiv \frac{P_v - P_{v,sat}}{P_{v,sat}} = 0.2 \tag{A.6}$$

The saturation pressure at the frost surface at −5 °C is 0.1033 kPa. Hence, the water vapor pressure at the frost surface becomes 0.1240 kPa. Thus, the mass transfer rate is:

$$\begin{aligned} m'' &= K_p(P_{v,a} - P_{v,fs}) = K_p(0.2009 - 0.1240) \\ &= 0.0769K_p = 0.0769K_p \end{aligned} \tag{A.7}$$

If one assumes that the air is saturated at the frost surface, the mass transfer rate is

$$\begin{aligned} m'' &= K_p(P_{v,a} - P_{v,fs}) = K_p(0.2009 - 0.1033) \\ &= 0.0976K_p \end{aligned} \tag{A.8}$$

Hence, the assumption that the air at the frost surface is saturated at the frost surface temperature results in 27% overprediction of the mass transfer rate.

References

[1] P.L.T. Brian, R.C. Reid, Y.T. Shah, Frost deposition on cold surfaces, Ind. Eng. Chem. Fundam. 9 (3) (1970) 375–380.
[2] P.L.T. Brian, R.C. Reid, I. Brazinsky, Cryogenic frost properties, Cryog. Technol. 5 (1969) 205–212.
[3] B.W. Jones, J.D. Parker, Frost formation with varying environmental parameters, J. Heat Transfer 97 (1975) 255–259.
[4] S.M. Sami, T. Duong, Mass and heat transfer during frost growth, in: ASHRAE Transactions, vol. 95 (Part 1, no. 3218), 1989 pp. 158–165.
[5] R. Le Gall, J.M. Grillot, Modeling of frost growth and densification, Int. J. Heat Mass Transfer 40 (13) (1997) 3177–3187.
[6] N.H. Fletcher, The Chemical Physics of Ice, Cambridge University Press, Cambridge, 1970 (Chapters 4 and 5).
[7] C.T. Sanders, The influence of frost formation and defrosting on the performance of air coolers, Ph.D. Thesis, Delft Technical University, 1974.
[8] V.P. Carey, Liquid–Vapor Phase Change Phenomena, Taylor & Francis, London, 1992 (Chapters 5, 6 and 9).

[9] Y. Hayashi, A. Aoki, S. Adachi, K. Hori, Study of frost properties correlating with frost formation types, J. Heat Transfer 99 (1977) 239–245.
[10] H.W. Schneider, Equation of the growth rate of frost forming on cooled surface, Int. J. Heat Mass Transfer 21 (1978) 1019–1024.
[11] S. Sengupta, S.A. Sherif, K.V. Wong, Empirical heat transfer and frost thickness correlations during frost deposition on a cylinder in cross-flow in the transfer regime, Int. J. Energy Res. 22 (1998) 615–624.
[12] S.A. Sherif, S.P. Raju, M.M. Padki, M.M. Chan, A semi-empirical transient method for modeling frost formation on a flat plate, Int. J. Refrig. 16 (5) (1993) 321–329.
[13] B. Na, Analysis of frost formation on the evaporator, Ph.D. Thesis, The Pennsylvania State University, 2001.
[14] A.R. Balkenende, H.J.A.P. Van de Boogaard, M. Scholten, N.P. Willard, Evaluation of different approaches to assess the surface tension of low-energy solids by means of contact angle measurement, Langmuir 14 (1998) 5907–5912.
[15] G.A. Somorjai, Introduction to surface chemistry and catalysis, John Wiley and Sons, New York, 1994 (Chapter 3).
[16] A.W. Adamson, A.P. Gast, Physical Chemistry of Surfaces, sixth ed., John Wiley and Sons, New York, 1997 (Chapters IX and X).
[17] P.G. Harraghy, J.M. Barber, Frost formation, Proc. Inst. Refrig. 83 (1987) 13–27.
[18] J. Min, R.L. Webb, Long-term wetting and corrosion characteristics of hot water treated aluminum and copper fin stocks, Int. J. Refrig. 25 (2002) 1054–1061.
[19] X.M. Wu, R.L. Webb, Investigation of the possibility of frost release from a cold surface, Exp. Therm. Fluid Sci. 24 (2001) 151–156.
[20] R.L. Webb, Standard nomenclature for mass transfer processes, in: ASHRAE Transactions, vol. 97 (part 2), 1991, pp. 114–118.